Seasonal influenza circulation patterns and projections for February 2026 to February 2027

John Huddleston[1], Jennifer Chang[1], Jover Lee[1], Philippa Steinberg[1], Trevor Bedford[1,2] & Richard A. Neher[3]

[1]Vaccine and Infectious Disease Division, Fred Hutchinson Cancer Center, Seattle, WA, USA, [2]Howard Hughes Medical Institute, Seattle, WA, USA, [3]Biozentrum, University of Basel, Basel, Switzerland

February 20, 2026

Abstract

This report details current seasonal influenza circulation patterns as of early February 2026 and was prepared for the Northern Hemisphere VCM on February 20, 2026. This is not meant as a comprehensive report, but is instead intended as particular observations that we've made that may be of relevance. Please also note that observed patterns reflect the GISAID database and may not be entirely representative of underlying dynamics. All analyses are based on the Nextstrain pipeline [1, 2] with continual updates posted to nextstrain.org/seasonal-flu. *In compliance with data sharing agreements, this public version of the report does not include raw serological measurements.* **A/H1N1pdm:** HA clade D.3.1.1 continues to grow globally, replacing C.1.9.3 and most other D.3.1 clades. Subclades within D.3.1.1 carrying HA1:139N or HA1:205K have started to grow in Europe and North America but remain at low frequencies elsewhere. Neutralization titers from human sera showed the highest antigenic advance for D.3.1.1, D.3.1:270A, and D.3.1.1:155E, while ferret serology showed little signal of antigenic advance for recent clades. We predicted that vaccine candidates from D.3.1.1 including A/Michigan/103/2025, A/Tokyo/EIS13-602/2025, and A/Tokyo/EIS13-863/2025 were antigenically closest to the predicted future H1N1pdm populations. **A/H3N2:** HA clade K is the dominant clade globally. In all regions where K and J.2.3 have cocirculated recently (North America, South America, and Europe), J.2.3 has a consistently lower fitness than K and its emerging haplotypes. Both human and ferret serological data indicated similarly high antigenic advance of clades K, J.2.4, and J.2.3. A subclade of J.2.4 with HA1:135N had the highest antigenic advance in ferrets and humans. We predicted that vaccine candidates from K like A/Darwin/1415/2025 were closest to the predicted future H3N2 populations. **B/Vic:** HA clade C.3.1 has circulated outside of the USA with most samples collected in Australia, Chile, and Brazil. However, we only estimate a consistently high growth advantage for C.3.1 in North America. A sibling clade of C.3.1 (C.3 with HA1:255P, 267V, and 197N substitutions) has reassorted with a different NA background and remains at low frequency. C.3.1 and other C.3 descendants with the HA1:197N substitution have the highest antigenic advance of any clade by ferret serological data.

Contents

Methods and Notes

Sequence data and subsampling

We base our analysis on sequence data available in GISAID as of February 19, 2026 and titer data available as of February 19, 2026. The availability of sequences varies greatly across time and geography and we try to minimize geographical and temporal bias by subsampling the data or analyzing different geographical regions separately when appropriate. While this subsampling reduces geographical biases, it doesn't remove this bias entirely.

Phylogenetic analysis

The database contains too many sequences to perform a comprehensive phylogenetic analysis of all available data. We hence subsample the data to at least 3000 sequences collected in the last 2 years. To minimize bias from differences in surveillance intensity, we evenly sample at most 2700 sequences (90%) across region, year and month bins for regions including North America, Oceania, China, South America, West Asia, Japan and Korea, Southeast Asia, Africa, and South Asia. For European data, we sample at most 300 sequences (10%) across country, year and month bins. Within each region/country, year, and month group, we prioritize sequences with corresponding antigenic data. For phylogenetic context, we include an additional 300 sequences collected prior to 2 years ago and as early as January 2016, evenly sampling by region and year. We also include all strains with titer measurements as a test or reference virus, to ensure that all titer data are available to observe in our interactive reports.

Parallel evolution, that is repeated occurrence of identical substitutions in different clades of the tree, is common in A/H3N2 and A/H1N1pdm. Such parallel evolution violates fundamental assumptions of common phylogeny software and can erroneously group distinct clades together if they share too many parallel changes. To avoid such artifacts, we mask sites with rampant parallelism prior to phylogeny inference.

Clades and subclades are assigned using a collection of "signature" mutations available at the GitHub repository github.com/nextstrain/seasonal-flu for each lineage via the following links:

- H1N1pdm HA
- H1N1pdm NA
- H3N2 HA
- H3N2 NA
- Vic HA
- Vic NA

Frequency and fitness estimates

Although phylogenetic analyses require a subset of all available sequences to reduce biases in the tree, we apply a non-phylogenetic method to estimate clade frequencies from all hemagglutinin (HA) sequences per lineage. We align all HA sequences to the lineage's reference sequence using Nextclade and obtain clade labels and amino acid substitutions per sequence [3]. From these Nextclade annotations per sequence, we jointly estimate the frequencies and relative growth advantages of each clade per geographic region in 14-day intervals using a hierarchical multinomial logistic regression

(MLR) model [4]. Multinomial logistic regression across n variants models the probability of a virus sampled at time t belonging to variant i as equal to its frequency $x_i(t)$ following

$$\Pr(X = i) = x_i(t) = \frac{p_i \exp(f_i\, t)}{\sum_j p_j \exp(f_j\, t)}.$$

A toy example of MLR fit to frequency data is shown in Figure 1.

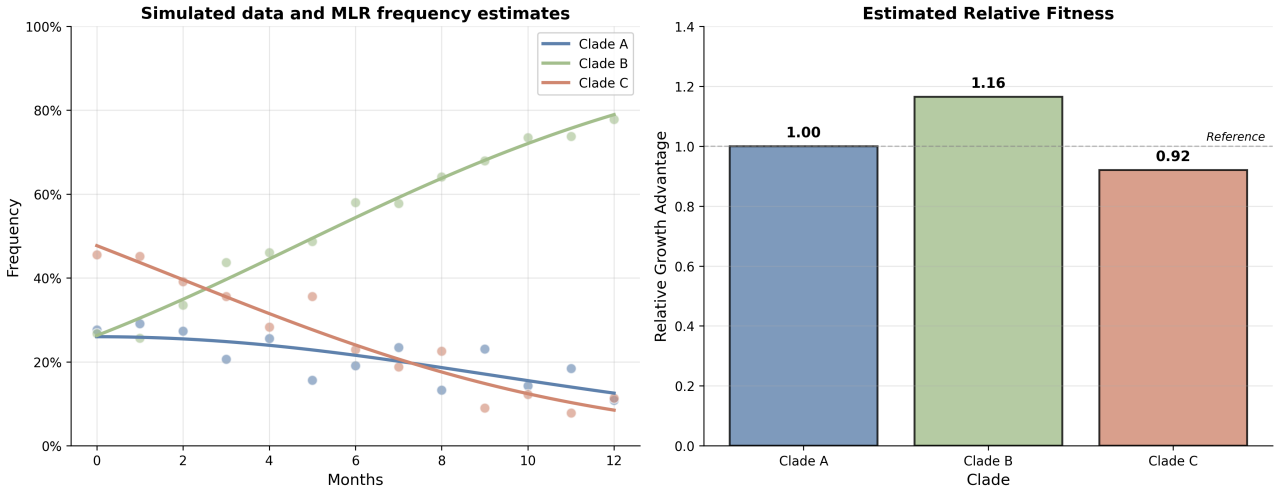

Figure 1. Demo of MLR model and directly estimating clade-level growth advantage from frequency dynamics.

Growth advantages reflect the advantage of each clade relative to a specific reference clade or "pivot" clade. Values less than 1 indicate lower fitness than the pivot clade and values greater than 1 indicate higher fitness. In addition to estimating region-specific growth advantages, the model estimates an average growth advantage and variance per clade across all regions which we report as the "hierarchical GA". The hierarchical GA is analogous to the local branching index in that it reflects the recent global success of each clade. The region-specific GA is analogous to a region-specific local branching index.

Antigenic analysis of ferret data

We summarize HI and FRA measurements provided by the WHO CCs in London, Melbourne, Atlanta, and Tokyo using our *substitution model* [5] which models log-titers as a sum of effects associated with amino acid differences between the sequences of the test and reference virus. In addition, the model allows for a serum (column) and a virus (row) effect. This model allows inference of titers for virus/serum pairs that have not been antigenically characterized and isolates effects consistently observed across many measurements from the noise inherent in individual measurements. We also plot individual and average normalized $\log_2$ titers per reference serum for test viruses in specific clades, to represent the raw antigenic data available for each influenza lineage.

In addition to the MLR-based growth advantages described above, we estimated the fitness of currently circulating strains using antigenic advance based on titer measurements from ferret sera [5]. High antigenic advance indicates groups of viruses with amino acid substitutions that are inferred to increase the antigenic distance from viruses without those substitutions.

High throughput human serology and antigenic analysis

Kikawa et al. [6] describes the generation of a library of 57 recently circulating H3N2 strains and 34 recently circulating H1N1pdm strains (Fig. 2). This work uses a high-throughput sequencing-based neutralization assay to measure neutralization titers for these 91 viruses against a panel of 302 human sera collected from individuals spanning from young children to elderly adults, drawn from four sites around the world and collected between July and November 2025. We apply the same 'titer model' as used for ferret data [5] to predict antigenic escape for strains that were not directly measured in the assay. In this report, we focus on neutralization titers for a subset of sera (N=243) that excludes post-vaccination serum samples.

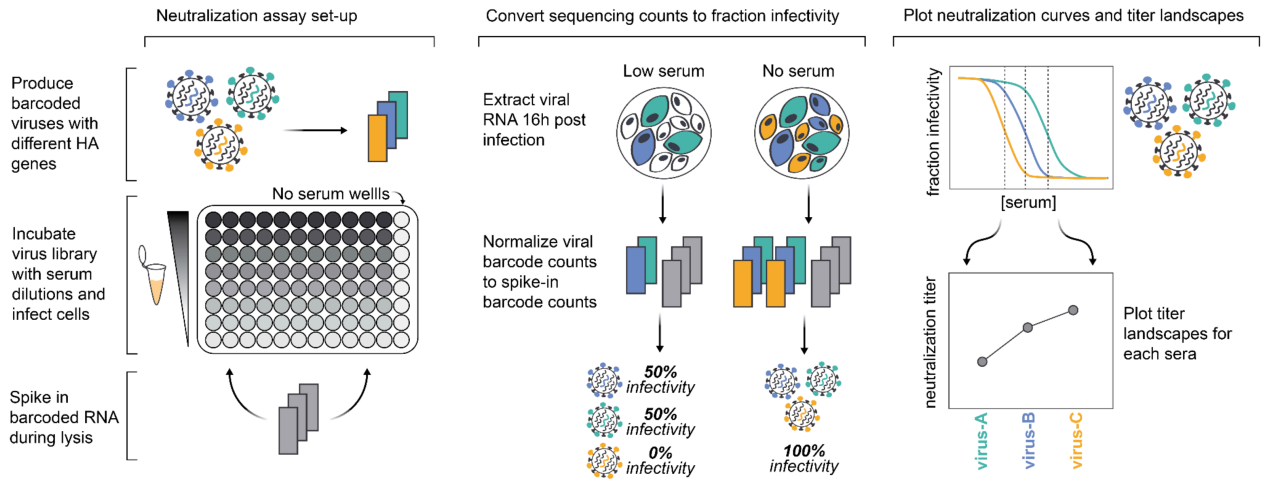

Figure 2. High-throughput sequencing-based neutralization assays enable rapid measurement of human serological responses across many viruses. Figure reproduced from Kikawa et al. [7].

Antigenic distance to the predicted future population

To rank vaccine candidates per subtype by their antigenic distance to the future, we integrated antigenic distance estimated from human or ferret serological data with predicted future frequencies estimated by the MLR model. The MLR model allows us to predict future frequencies of emerging haplotypes per geographic region. Our titer substitution model [5] estimates the antigenic effect of each HA1 substitution between reference and test viruses. For each reference virus used in ferret cell HI experiments (vaccine candidates), we calculated the average antigenic distance between that candidate's HA1 amino acid sequence and the corresponding HA1 sequence for each virus in each combination of emerging haplotype and geographic region. We calculated each pairwise antigenic distance between the candidate and another virus sequence as the sum of antigenic effects associated with the substitutions between the two viral HA1 sequences. We calculated a weighted average antigenic distance to the future by multiplying the predicted future frequency of each haplotype in a given region (e.g., Fig. 4) by the average antigenic distance for that haplotype/region combination. Finally, we averaged these estimates across regions to get the weighted average antigenic distance for the vaccine strain to the predicted future population. Candidates with the lowest distances are predicted to be the best representatives of the future population.

A/H1N1pdm

Summary

HA clade D.3.1.1 continues to grow globally, replacing C.1.9.3 and most other D.3.1 clades (Figs. 3 and 4). Subclades within D.3.1.1 carrying HA1:139N or HA1:205K have started to grow in Europe and North America but remain at low frequencies elsewhere (Fig. 4). We currently estimate that these two subclades have a higher fitness in Europe than the ancestral D.3.1.1 clade (Fig. 5). D.3.1:270A is a polyphyletic group with recurrent emergence in Maldives, South Australia, USA/Japan/Sydney/Malaysia and different NAs for each HA clade. This group has a high growth advantage only in Oceania with a value comparable to D.3.1.1 and higher than ancestral D.3.1 viruses (Fig. 5). HA1:G155E also appear multiple times within D.3.1.1 including a subclade circulating primarily in Europe and another primarily in Canada. Although this substitution reduces titers in ferrets and humans in serological assays, 155E remains at low frequencies globally (Fig. 4) with a low growth advantage relative to D.3.1.1 (Fig. 5).

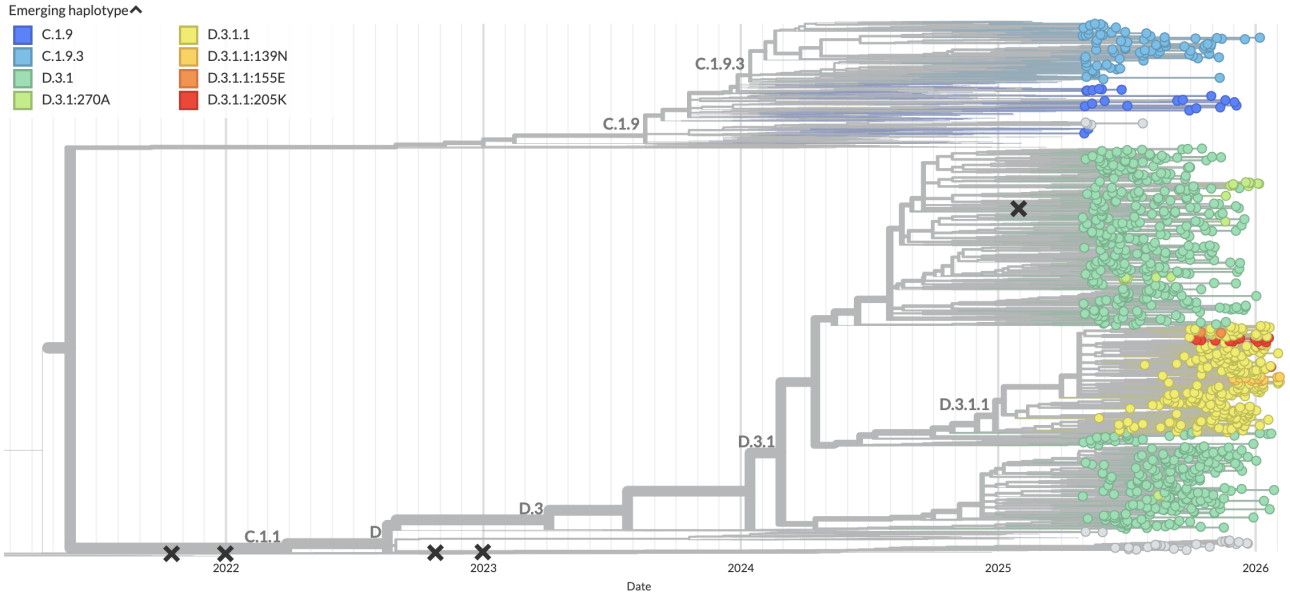

Figure 3. Time-resolved A/H1N1pdm phylogeny colored by clade and filtered to strains collected since May 1, 2025. View on nextstrain.org.

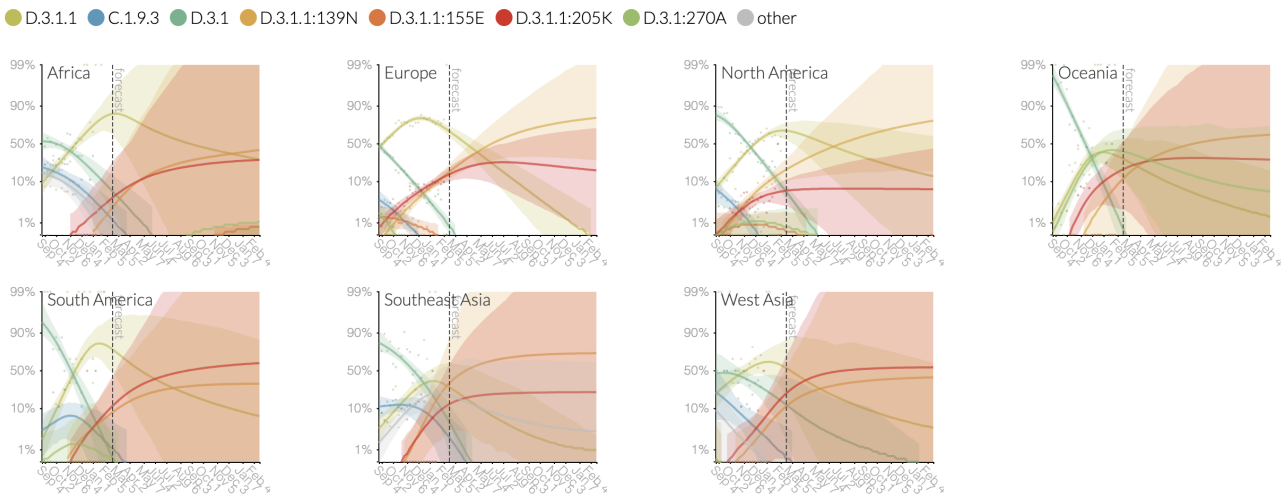

Figure 4. Clade frequencies by region estimated by a multinomial logistic regression (MLR) model. Lines show the median frequency (± 95% HPDIs) and 1-year forecasts estimated under an assumption of exponential growth. Colored points indicate frequency estimates from the raw data binned into biweekly intervals. View on Nextstrain.

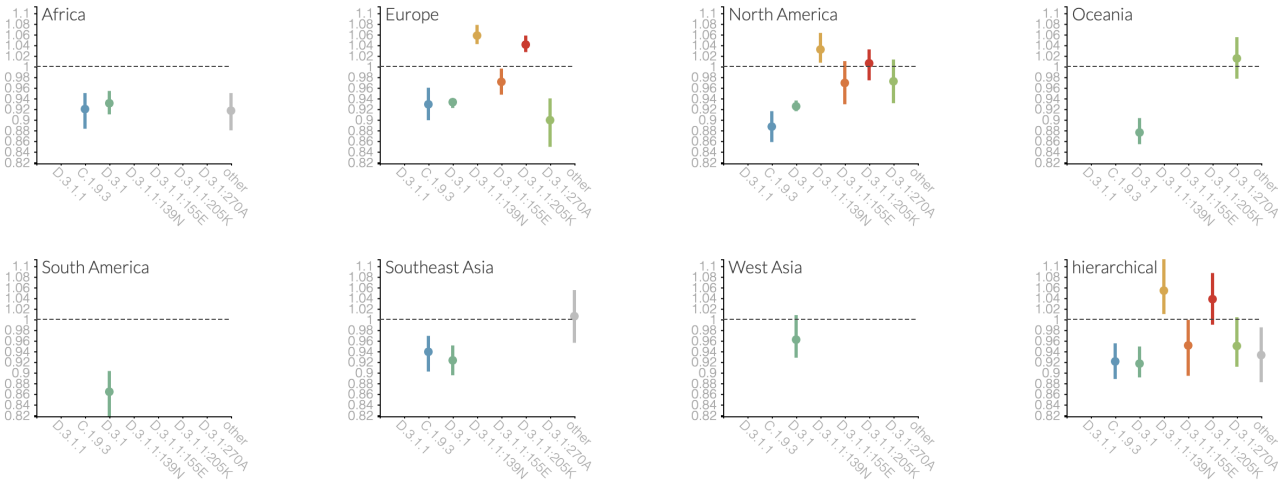

Figure 5. Growth advantages per clade by region as estimated by a MLR model. The "hierarchical" advantage represents the global average fitness per clade. The dashed vertical line at x=1 indicates the growth advantage of the pivot clade. Clades with growth advantages greater than 1 have a higher fitness than the pivot. Colored points indicate the median growth advantage per clade and location (± 95% HPDIs). View on Nextstrain.

Antigenic properties from ferret serology

Viruses with 155E and 155R substitutions continue to show greater antigenic distances across all genetic backgrounds (Fig. 6). Otherwise, we do not observe differences in antigenic advance among clades from ferret HI data.

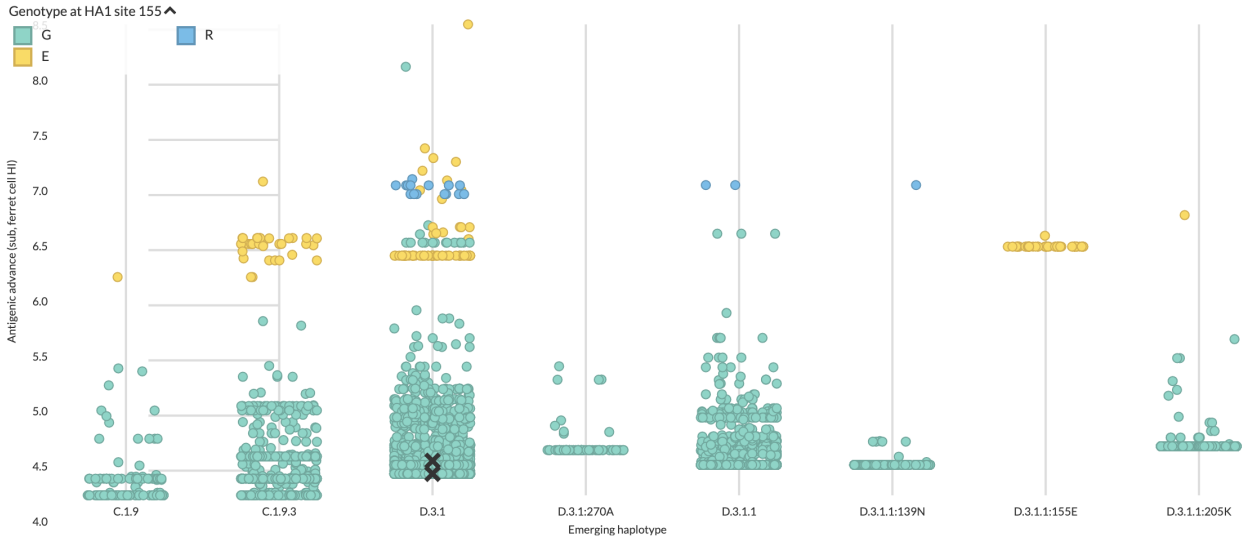

Figure 6. Antigenic advance across clades estimated from ferret-based HI data [5] for samples collected since May 1, 2025. View on nextstrain.org.

[Raw ferret data redacted]

Antigenic properties from human serology

Caroline Kikawa from the lab of Jesse Bloom has measured neutralization titers against a selection of recent A(H3N2) and A(H1N1pdm) strains for several sera panels (302 sera in total – see methods summary at the beginning of the report). Her results are available in a preprint posted on bioRxiv [6] and summarized in the figures below.

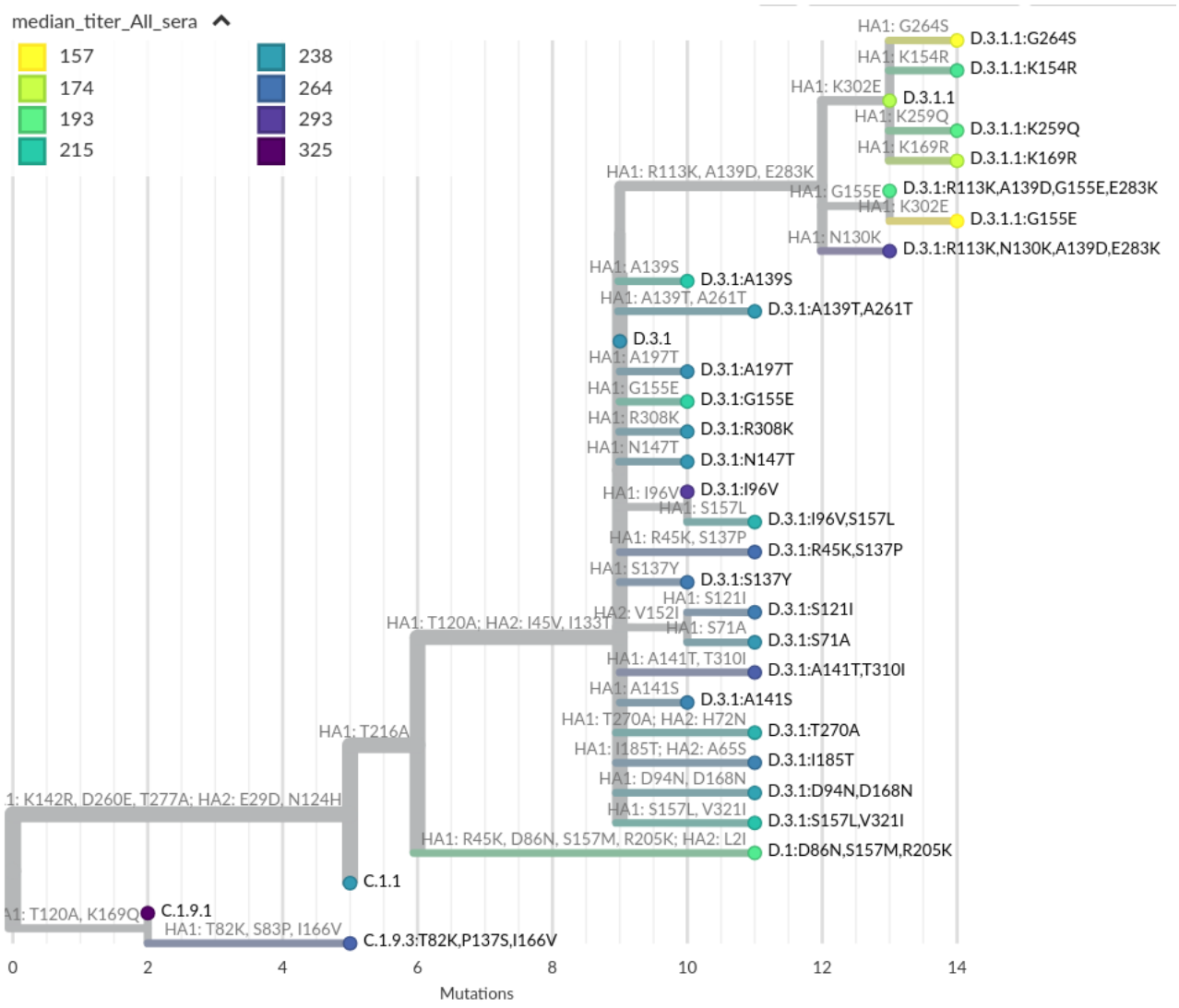

Figure 7. Tree summarizing the A(H1N1pdm) strains used by Kikawa et al [6] and the median titer across all sera.

Titer models fit to these neutralization titers show distinct antigenic advancement of clades D.3.1, D.3.1:270A, and D.3.1.1 relative to C.1.9.3 that we did not observe in ferret HI data (Fig. 8). We found the highest antigenic advance for D.3.1.1 and its subclade with the HA1:155E substitution. Unlike the results for ferret serological data, these results support the hypothesis that immune escape caused by HA1 substitutions have contributed to the recent success of D.3.1 and D.3.1.1.

Figure 8. Antigenic advance across clades estimated from human-based neutralization data [6] for samples collected since May 1, 2025. View on nextstrain.org.

Comparing viral fitness forecasts and antigenic phenotype

To understand the relationship between viral fitness estimated from frequency dynamics (growth advantages from the MLR model) vs from experimental data (antigenic advancement), we plotted the growth advantage of each recent emerging haplotype against the corresponding median antigenic advance of sequences in that haplotype based on human or ferret serological data. Human antigenic advance corresponds with estimated fitness in nature better than ferret antigenic advance does (Fig. 9). For example, greater antigenic advance for D.3.1.1 clades compared to C.1.9.3 and D.3.1 generally corresponds with higher fitness. We estimated a strong effect of D.3.1:270A on human immune escape which does not match the recent global success of that haplotype. However, the antigenic advance of this haplotype may explain its rise to dominance in Oceania over the last six months. In contrast, we see no distinction between most recent clades by antigenic advance from ferrets. The exception is D.3.1.1:155E which has the highest antigenic advance in humans and ferrets and has one of the lowest fitnesses. From human sera, we estimate that HA1:155E reduces titers by less than 1 $\log_2$ unit relative to D.3.1.1. From ferret sera, we estimate a stronger reduction of 2 $\log_2$ units.

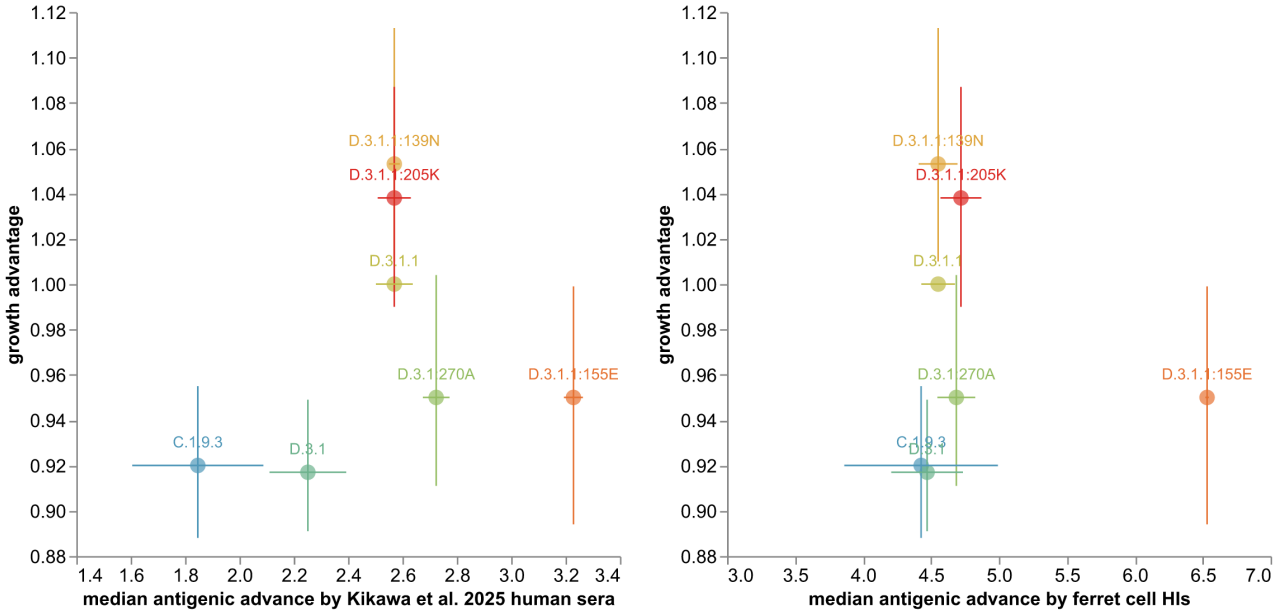

Figure 9. Growth advantage by antigenic advance per clade estimated with a titer substitution model [5] for human-based neutralization data [6] (left) and ferret-based cell HI data (right). Growth advantages shown as median +/- 95% HPDIs. Antigenic advance shown as median +/- 1 standard deviation across all sequences in a given clade.

Finally, we ranked the available vaccine candidates by their antigenic distance to the predicted future H1N1pdm population as described in the Methods. We found that viruses from D.3.1.1 including A/Michigan/103/2025, A/Tokyo/EIS13-602/2025, and A/Tokyo/EIS13-863/2025 were closest to the predicted future (0.01 $\log_2$ units away on average), followed by other viruses in D.3.1 (0.29 $\log_2$ units) including the current Southern Hemisphere vaccine, A/Missouri/11/2025 (Fig. 10). In contrast to these distances based on human antigenic advance, distances based on ferret antigenic advance did not distinguish between most viruses descending from C.1.1 (Fig. 11).

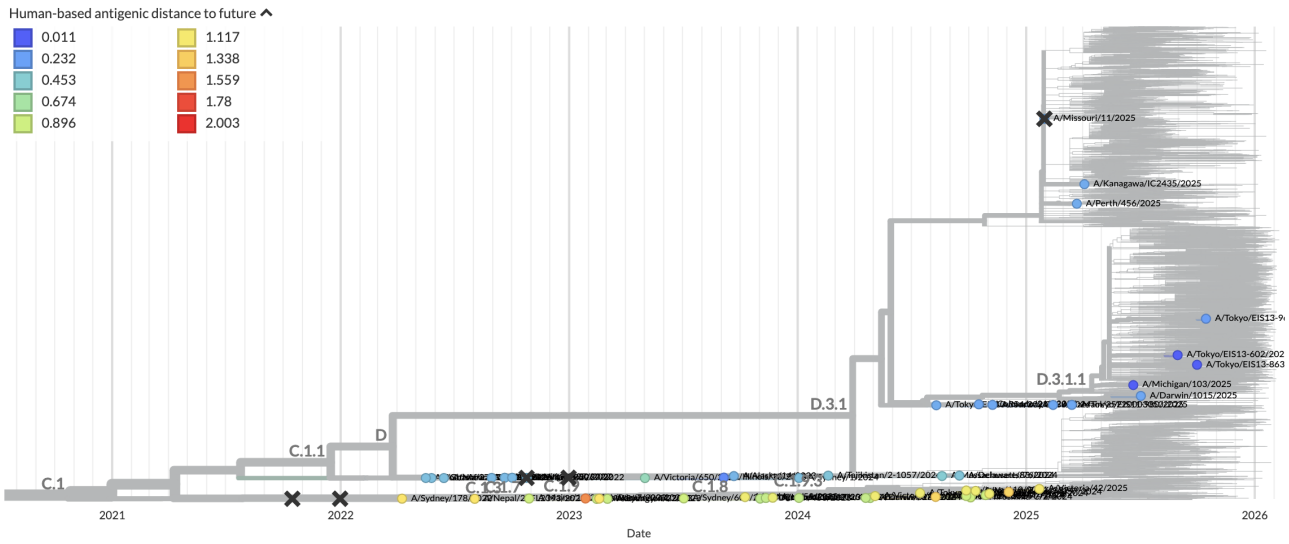

Figure 10. Weighted average antigenic distance to the future population per reference virus using human-based neutralization data. For each reference virus, we calculated the average antigenic distance between that virus's HA1 amino acid sequence and the corresponding HA1 sequences for viruses from each emerging haplotype and geographic region. The pairwise antigenic distance between viruses was based on the HA1 substitutions between them and antigenic weights per substitution estimated with a titer substitution model [5] fit to human-based neutralization data [6]. View on nextstrain.org.

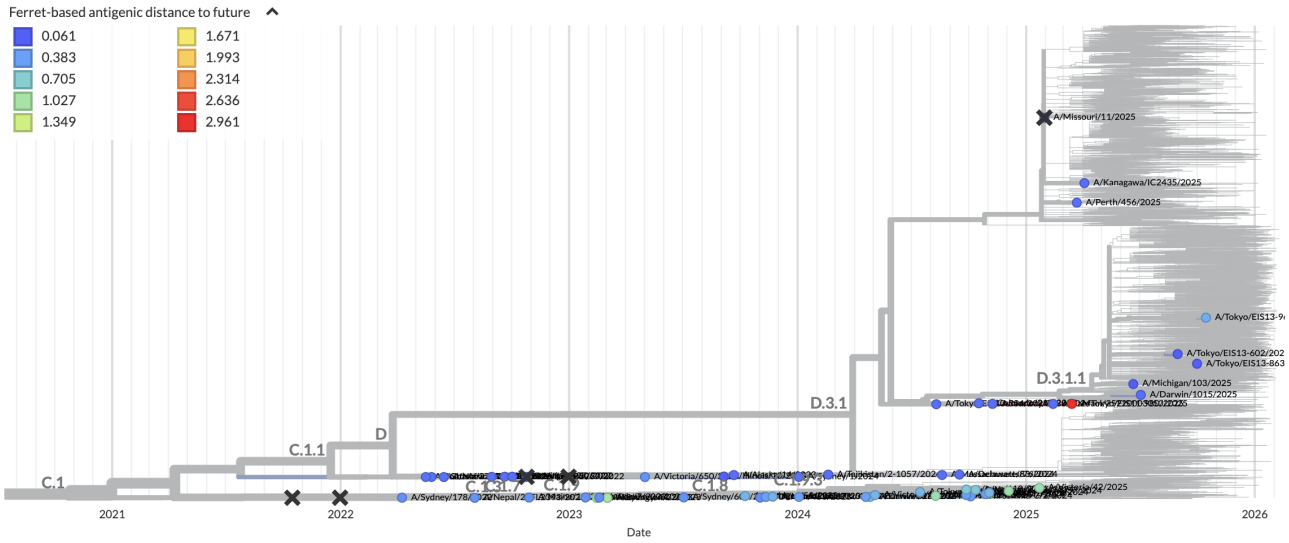

Figure 11. Weighted average antigenic distance to the future population per reference virus using ferret-based cell HI data. For each reference virus, we calculated the average antigenic distance between that virus's HA1 amino acid sequence and the corresponding HA1 sequences for viruses from each emerging haplotype and geographic region. The pairwise antigenic distance between viruses was based on the HA1 substitutions between them and antigenic weights per substitution estimated with a titer substitution model [5] fit to ferret-based cell HI data. View on nextstrain.org.

A/H3N2

Summary

HA clade K is the dominant clade globally (Figs. 12 and 13). Multiple new haplotypes continue to emerge within K, including K:80K, K:145N, K:223I, and K:328S. All of these emerging haplotypes except K:80K show signs of slightly higher fitness globally than ancestral K (Fig. 14). Inferred growth rates of different haplotypes vary regionally without a clear global successor to K yet. For example, K:145N and K:80K have the highest growth rates among haplotypes in Oceania. K:223I dominates other haplotypes in West Asia and K:328S dominates in Japan and Korea. Both HA1:145N and 223I substitutions have appeared many times against the K background without a single representative clade. In all regions where K and J.2.3 have cocirculated recently (North America, South America, and Europe), J.2.3 has a consistently lower fitness than K and its emerging haplotypes.

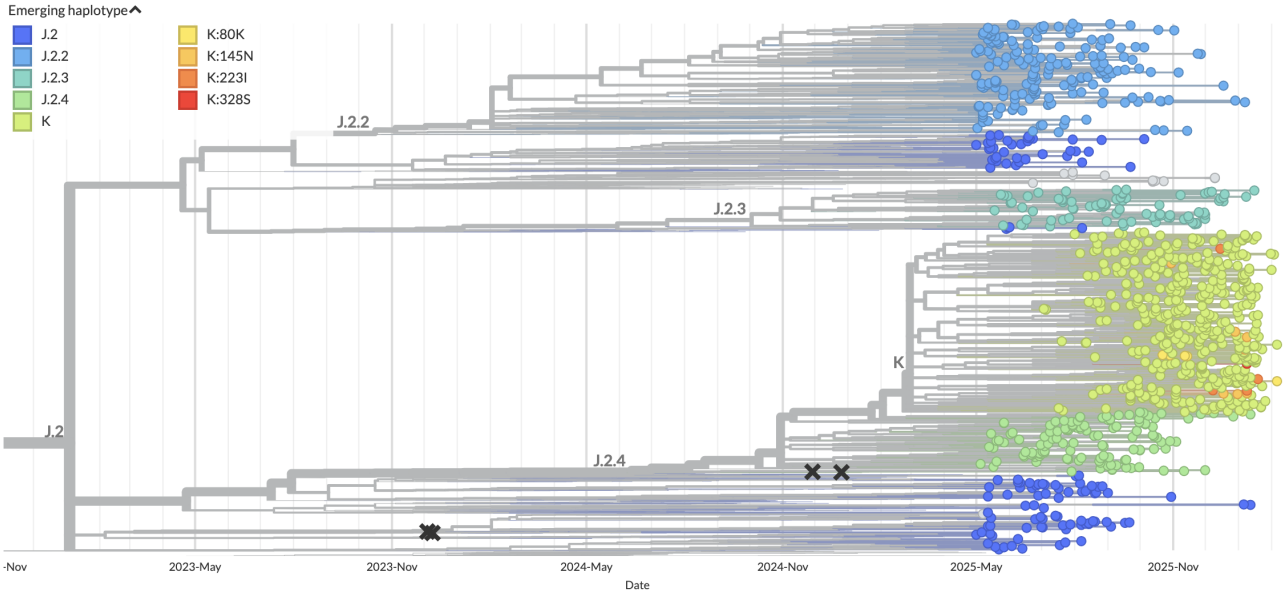

Figure 12. Time-resolved A/H3N2 phylogeny colored by clade and filtered to strains collected since May 1, 2025 View on nextstrain.org.

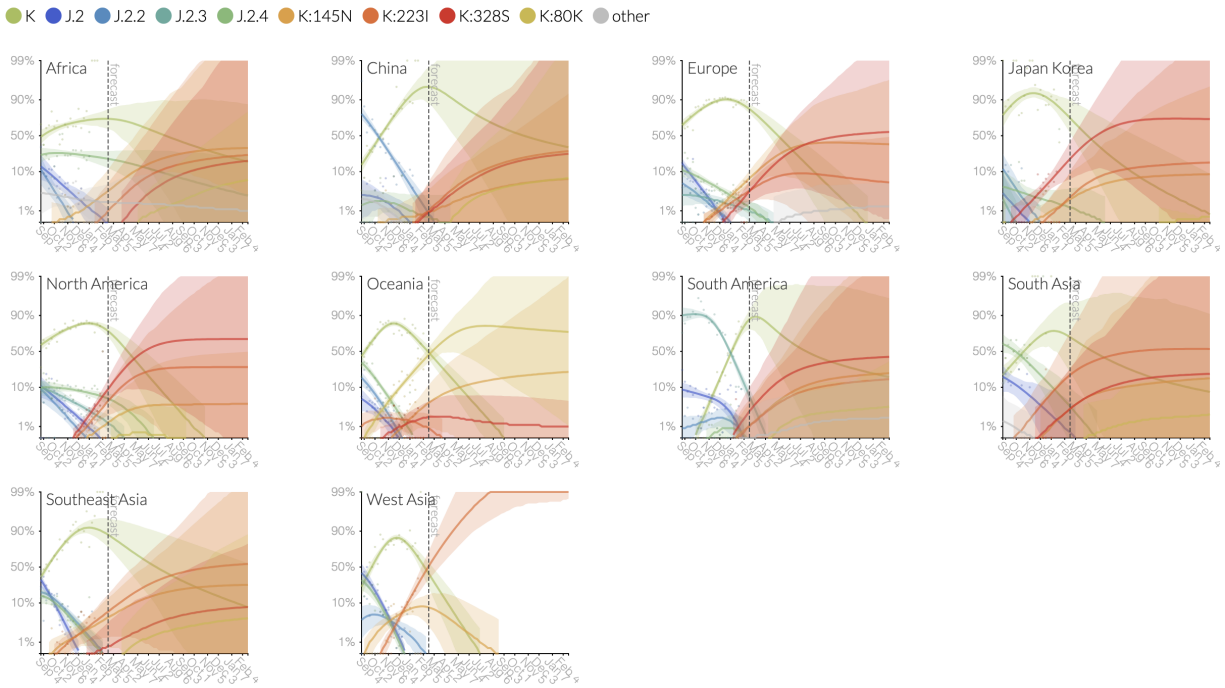

Figure 13. Clade frequencies by region estimated by a multinomial logistic regression (MLR). Lines show the median frequency (± 95% HPDIs) and 1-year forecasts. Colored points indicate frequency estimates from the raw data. View on Nextstrain.

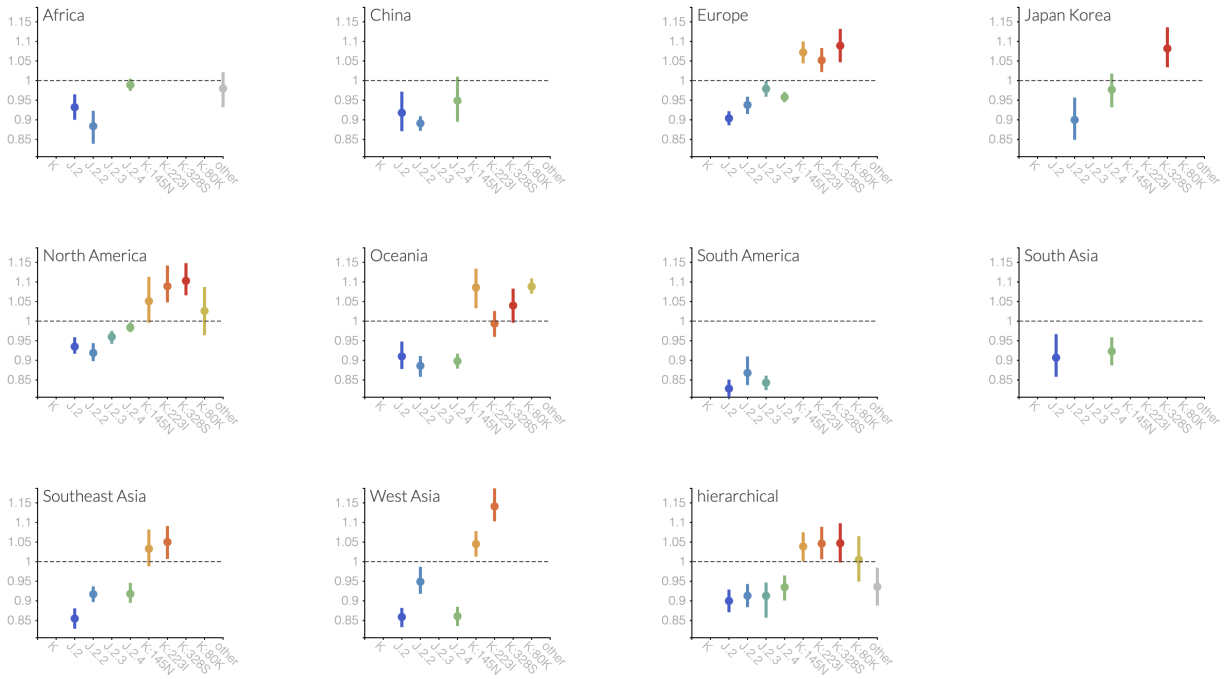

Figure 14. Growth advantages (median ± 95% HPDIs) per clade by region as estimated by a MLR model. The "hierarchical" advantage represents the global average fitness per clade. Advantages are relative to a pivot clade with a fixed advantage of 1. View on Nextstrain.

Antigenic properties from ferret serology

Synthesizing all ferret measurements into our titer substitution model, we find the highest antigenic advance for J.2.3, K and its subclades, and a subset of J.2.4 viruses with a HA1:135N substitution (Fig. 15). Emerging haplotypes within K all have similar antigenic advances to the ancestral clade.

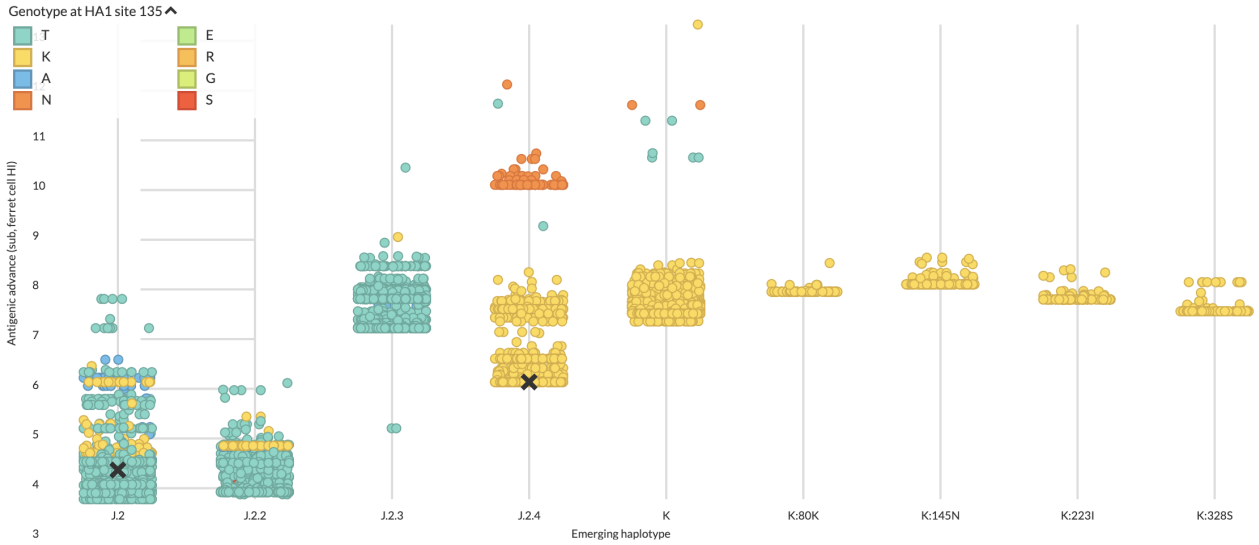

Figure 15. Antigenic advance per clade estimated from ferret-based HI data [5] for samples collected since May 1, 2025. In each panel, points represent individual HA sequences whose overall antigenic advance has been inferred from a titer model based on the corresponding raw serological data. Points are colored by their genotype at position HA1 135 to highlight the antigenic advance of J.2.4 strains with HA1:135N. View on nextstrain.org.

[Raw ferret data redacted]

Antigenic properties from human serology

Caroline Kikawa from the lab of Jesse Bloom has measured neutralization titers against a selection of recent A(H3N2) and A(H1N1pdm) strains for several sera panels (302 sera in total – see methods summary at the beginning of the report). Her results are available in a preprint posted on bioRxiv [6] and summarized in the figures below.

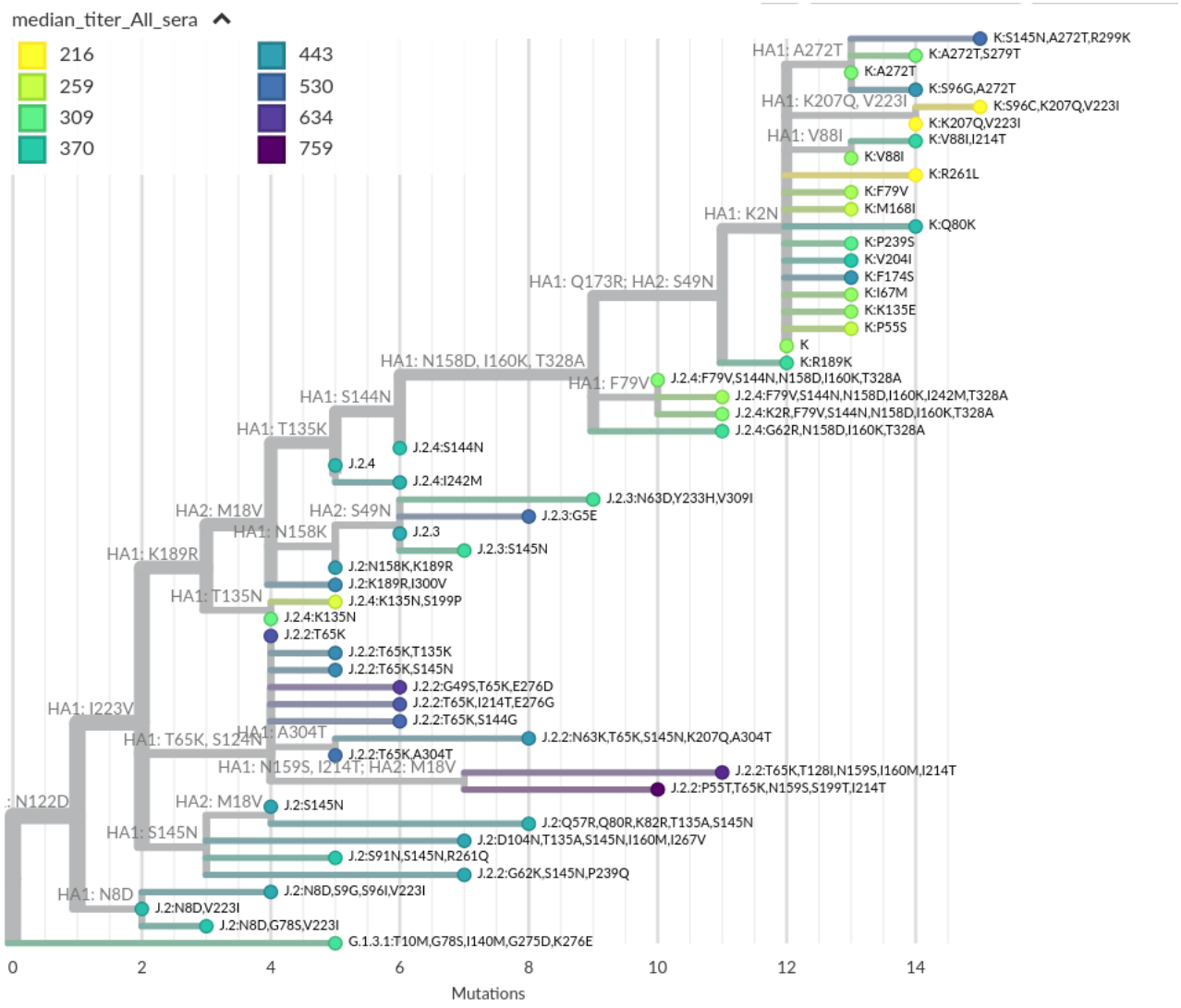

Figure 16. Tree summarizing the A(H3N2) strains used by Kikawa et al [6] and the median titer across all sera.

Titer models fit to these neutralization titers show similarly high antigenic advance for J.2.3 and K as found with ferret HI data (Fig. 17). Human titers show the same high antigenic advance of J.2.4:135N and also a similar effect of J.2.4 viruses with 79V and all K-defining substitutions except for HA1:173Q. We also noted a 2-fold range among antigenic advance values for K viruses, indicating that the genetic diversity in this clade corresponds to greater potential for escape from human immunity.

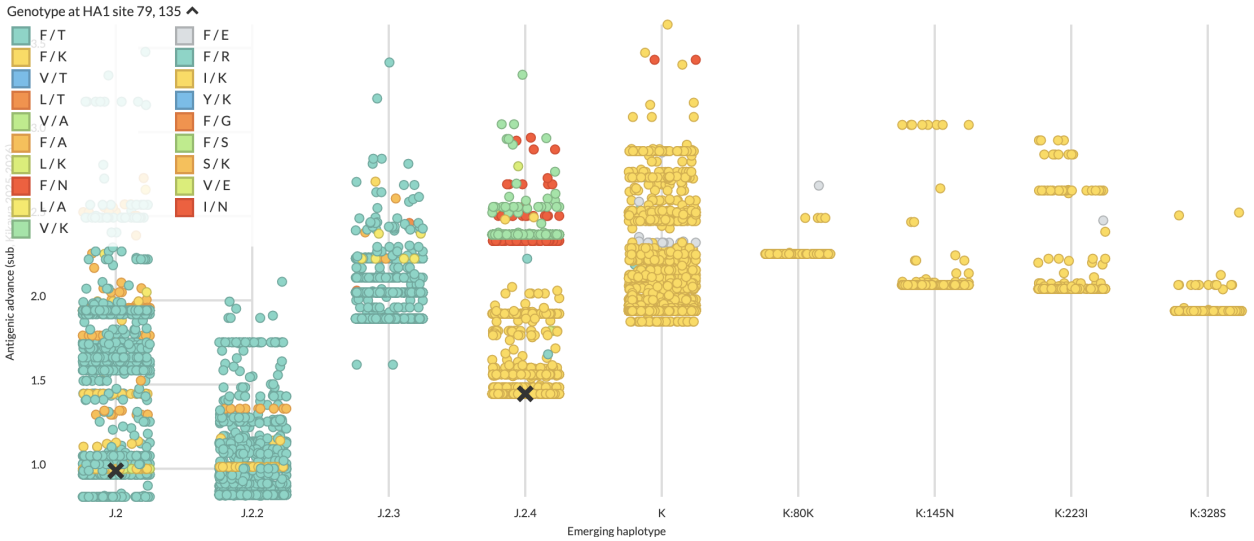

Figure 17. Antigenic advance across clades estimated from human-based neutralization data [6] for samples collected since May 1, 2025. Points are colored by their genotype at positions HA1 79 and 135 to highlight the antigenic advance of J.2.4 strains with HA1:135N or HA1:79V. View on nextstrain.org.

Comparing viral fitness forecasts and antigenic phenotype

To understand the relationship between viral fitness estimated from sequence data alone (growth advantages from the MLR model) or from experimental data (antigenic advance), we plotted the growth advantage of each recent emerging haplotype against the corresponding median antigenic advance of sequences in that haplotype based on human or ferret serological data. Most clades except for J.2 and J.2.2 appear similarly antigenically advanced based on both human and ferret serological measurements, without a clear correlation between higher recent fitness and higher antigenic advance (Fig. 18). Notably, K:80K has the highest antigenic advance for humans. This clade has not circulated much outside of Oceania yet, but in Oceania it has one of the highest estimated fitnesses.

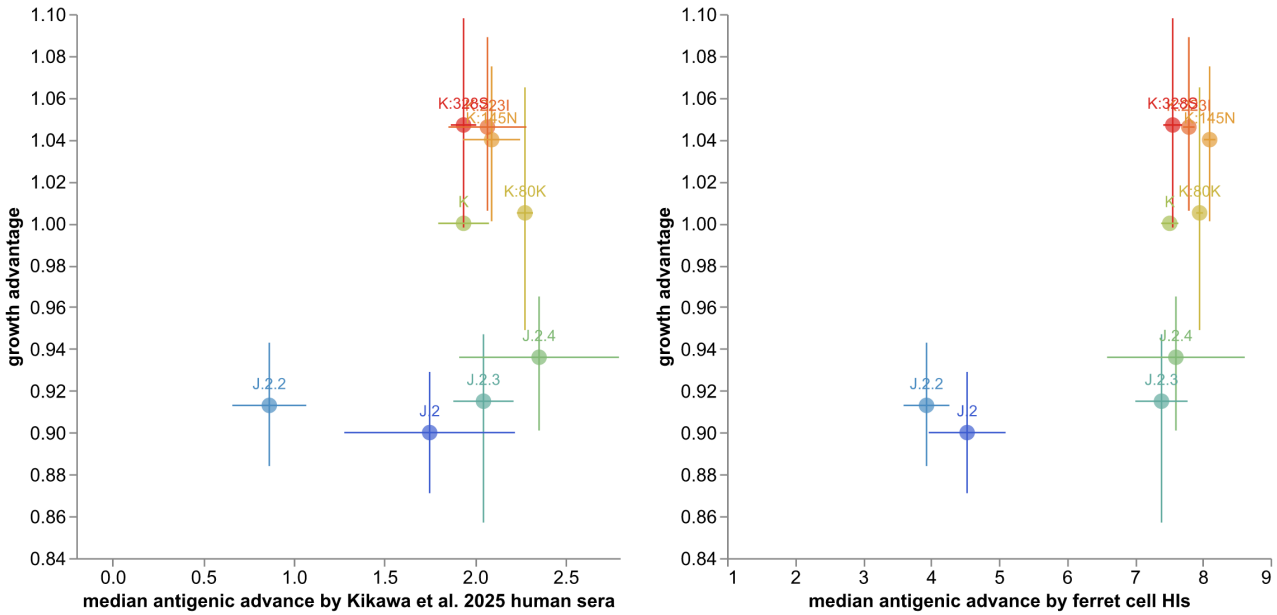

Figure 18. Growth advantage by antigenic advance per clade estimated with a titer substitution model [5] for human-based neutralization data [6] (left) and ferret-based cell HI data (right). Growth advantages shown as median +/- 95% HPDIs. Antigenic advance shown as median +/- 1 standard deviation across all sequences in a given clade.

Finally, we ranked the available vaccine candidates by their antigenic distance to the predicted future H3N2 population as described in the Methods. Results from both human and ferret antigenic models found that K reference viruses like A/Darwin/1415/2025 were closest to the predicted future (Figs. 19 and 20). Based on human serology, K reference viruses were all 0.11 $\log_2$ units from the predicted future population on average. In contrast, A/DistrictOfColumbia/27/2023 was 1.21 $\log_2$ units (about 2-fold) from the future and A/Sydney/1359/2024 was 0.51 $\log_2$ units away.

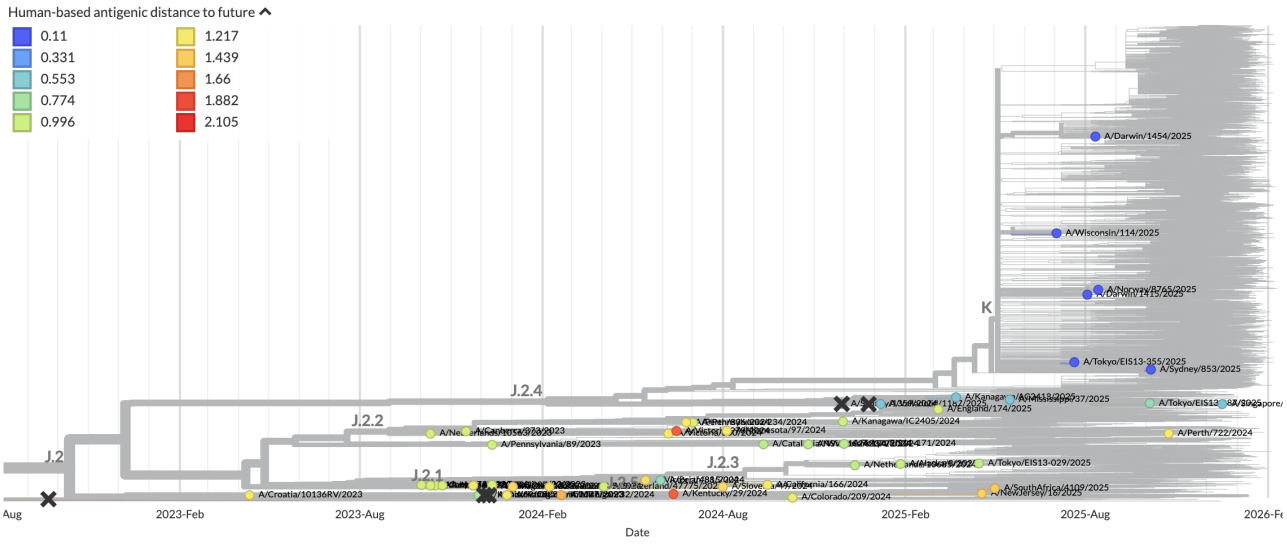

Figure 19. Weighted average antigenic distance to the future population per reference virus using human-based neutralization data. For each reference virus, we calculated the average antigenic distance between that virus's HA1 amino acid sequence and the corresponding HA1 sequences for viruses from each emerging haplotype and geographic region. The pairwise antigenic distance between viruses was based on the HA1 substitutions between them and antigenic weights per substitution estimated with a titer substitution model [5] fit to human-based neutralization data [6]. View on nextstrain.org.

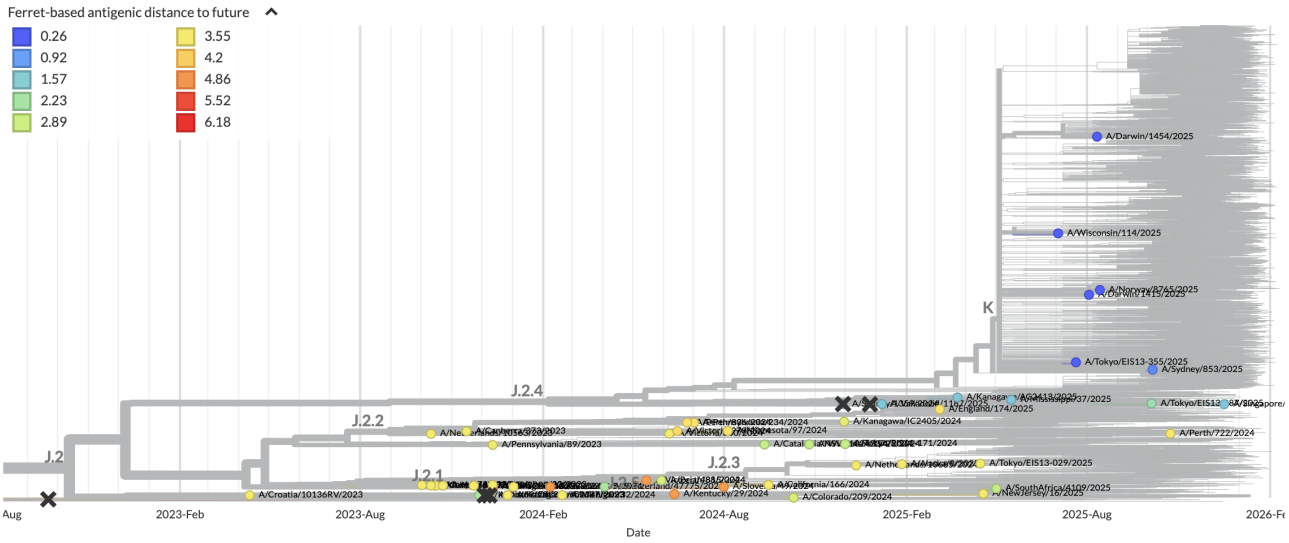

Figure 20. Weighted average antigenic distance to the future population per reference virus using ferret-based cell HI data. For each reference virus, we calculated the average antigenic distance between that virus's HA1 amino acid sequence and the corresponding HA1 sequences for viruses from each emerging haplotype and geographic region. The pairwise antigenic distance between viruses was based on the HA1 substitutions between them and antigenic weights per substitution estimated with a titer substitution model [5] fit to ferret-based cell HI data. View on nextstrain.org.

B/Vic

Summary

Few B/Victoria sequences have been collected in the last 6 months outside of North America (Fig. 21). HA clade C.3.1 has circulated outside of the USA with most samples collected in Australia, Chile, and Brazil (Fig. 22). However, we only estimate a consistently high growth advantage for C.3.1 in North America (Fig. 23). A sibling clade of C.3.1 (C.3 with HA1:255P, 267V, and 197N substitutions) has reassorted with a different NA background and remains at low frequency. HA clade C.5.1 continues to decline in frequency, while C.5.6 and C.5.7 co-circulate in all regions with recent sequence data (Fig. 22). An emerging subclade of C.5.6 with HA1:75E is at moderate frequency in China and Oceania (Fig. 22), but we only observe positive growth rates for this clade in Oceania (Fig. 23).

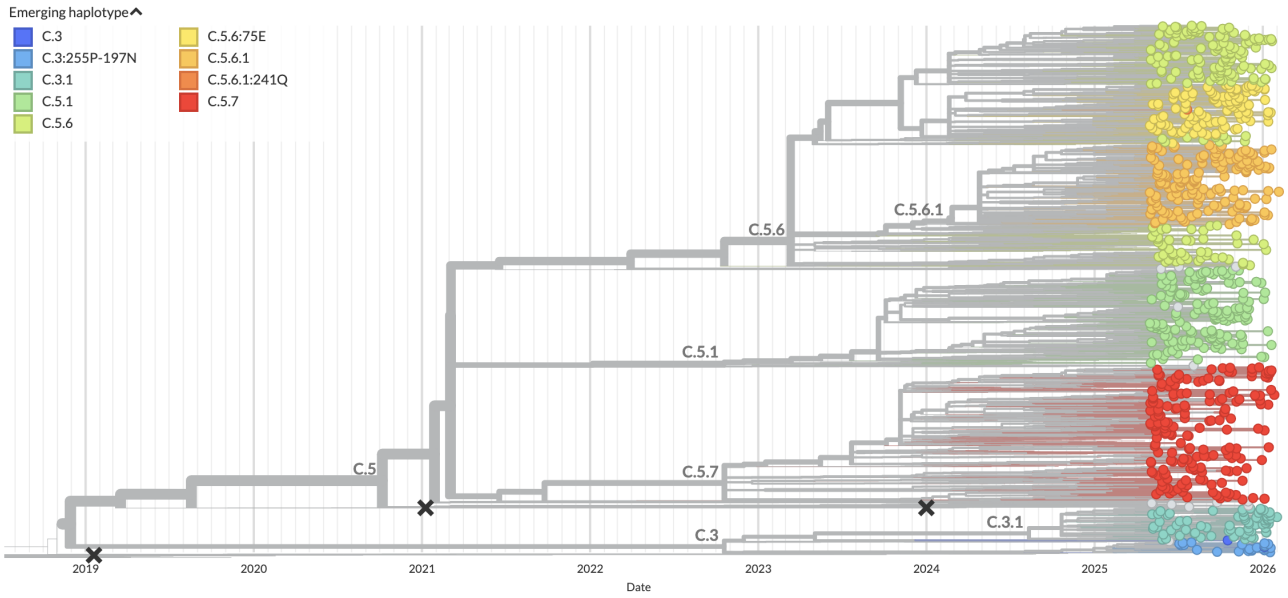

Figure 21. Time-resolved B/Victoria phylogeny colored by clade and filtered to strains collected since May 1, 2025. View on nextstrain.org.

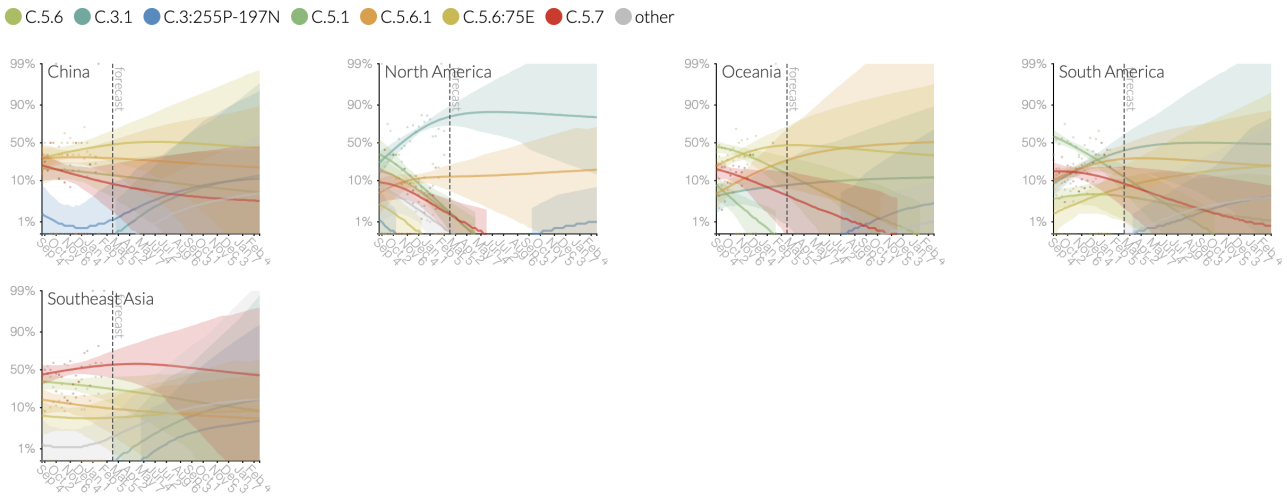

Figure 22. Clade frequencies by region estimated by a multinomial logistic regression (MLR). Lines show the median frequency (± 95% HPDIs) and 1-year forecasts. Colored points indicate frequency estimates from the raw data. View on Nextstrain.

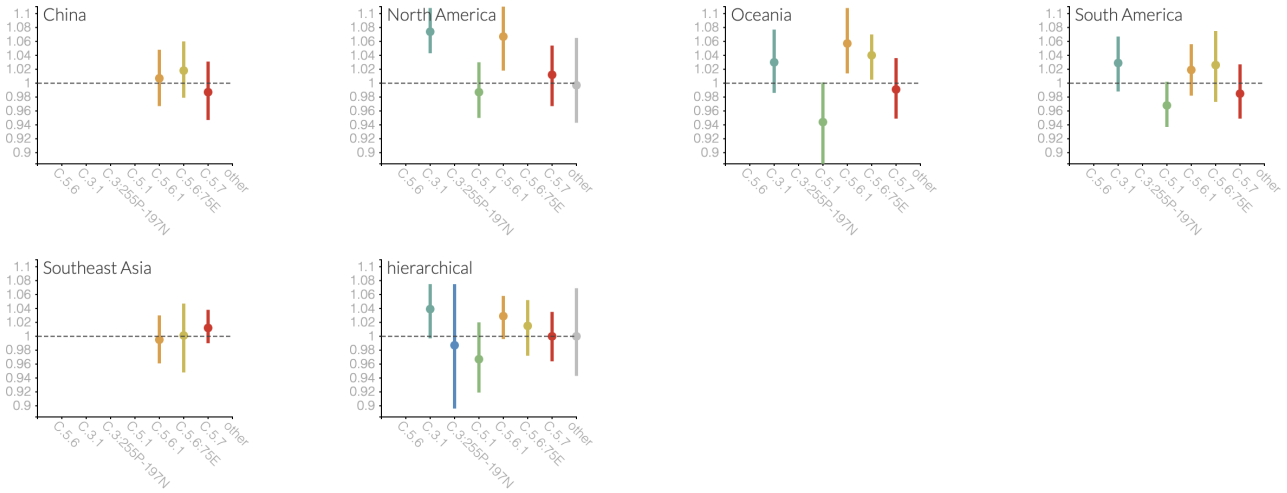

Figure 23. Growth advantages (median ± 95% HPDIs) per clade by region as estimated by a MLR model. The "hierarchical" advantage represents the global average fitness per clade. Advantages are relative to a pivot clade with a fixed advantage of 1. View on Nextstrain.

Antigenic properties from ferret serology

C.3.1 and other C.3 descendants with the HA1:197N substitution have the highest antigenic advance of any clade by ferret HI (Fig. 24).

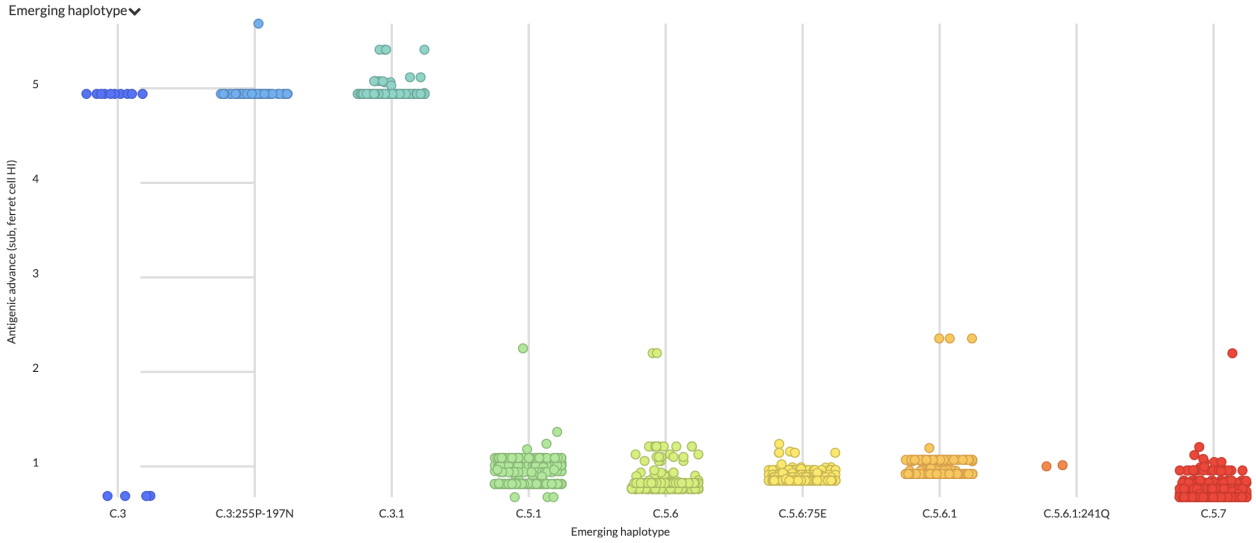

Figure 24. Antigenic advance per clade estimated from ferret-based HI data [5] for samples collected since May 1, 2025. View on nextstrain.org.

[Raw ferret data redacted]

Acknowledgments

This work is made possible by the timely sharing of influenza virus sequence data through GISAID. A table acknowledging each individual data contributor to the analysis on nextstrain.org/seasonal-flu can be found online at nextstrain.org/seasonal-flu. We thank the Influenza Division at the US Centers for Disease Control and Prevention, the Victorian Infectious Diseases Reference Laboratory at the Australian Peter Doherty Institute for Infection and Immunity, the Influenza Virus Research Center at the Japan National Institute of Infectious Diseases, the Crick Worldwide Influenza Centre at the UK Francis Crick Institute, Jesse Bloom and his lab, for data sharing and feedback. We thank Caroline Kikawa, Andrea Loes, Jesse Bloom and colleagues for contributing human serology data. We thank David Wentworth, Rebecca Kondor and Vivien Dugan for insight regarding analysis directions.

References

1. Neher RA, Bedford T (2015) nextflu: real-time tracking of seasonal influenza virus evolution in humans. Bioinformatics 31: 3546–3548.
2. Hadfield J, Megill C, Bell SM, Huddleston J, Potter B, et al. (2018) Nextstrain: real-time tracking of pathogen evolution. Bioinformatics 34: 4121–4123.
3. Aksamentov I, Roemer C, Hodcroft EB, Neher RA (2021) Nextclade: clade assignment, mutation calling and quality control for viral genomes. Journal of Open Source Software 6: 3773.
4. Abousamra E, Figgins M, Bedford T (2024) Fitness models provide accurate short-term forecasts of SARS-CoV-2 variant frequency. PLoS Comput Biol 20: e1012443.
5. Neher RA, Bedford T, Daniels RS, Russell CA, Shraiman BI (2016) Prediction, dynamics, and visualization of antigenic phenotypes of seasonal influenza viruses. Proc Natl Acad Sci USA 113: E1701–E1709.
6. Kikawa C, Huddleston J, Turner SA, Loes AN, Liu J, et al. (2026) Near real-time data on the human neutralizing antibody landscape to influenza virus as of early 2026 to inform vaccine-strain selection. bioRxiv .
7. Kikawa C, Huddleston J, Loes AN, Turner SA, Lee J, et al. (2025) Near real-time data on the human neutralizing antibody landscape to influenza virus to inform vaccine-strain selection in September 2025. bioRxiv : 2025.09.06.674661.